

Mid-Rapidity Direct-Photon Production in p+p Collisions at $\sqrt{s} = 200$ GeV

S.S. Adler,⁵ S. Afanasiev,¹⁷ C. Aidala,⁵ N.N. Ajitanand,⁴³ Y. Akiba,^{20,38} J. Alexander,⁴³ R. Amirikas,¹² L. Aphecetche,⁴⁵ S.H. Aronson,⁵ R. Averbeck,⁴⁴ T.C. Awes,³⁵ R. Azmoun,⁴⁴ V. Babintsev,¹⁵ A. Baldisseri,¹⁰ K.N. Barish,⁶ P.D. Barnes,²⁷ B. Bassalleck,³³ S. Bathe,³⁰ S. Batsouli,⁹ V. Baublis,³⁷ A. Bazilevsky,^{39,15} S. Belikov,^{16,15} Y. Berdnikov,⁴⁰ S. Bhagavatula,¹⁶ J.G. Boissevain,²⁷ H. Borel,¹⁰ S. Borenstein,²⁵ M.L. Brooks,²⁷ D.S. Brown,³⁴ N. Bruner,³³ D. Bucher,³⁰ H. Buesching,³⁰ V. Bumazhnov,¹⁵ G. Bunce,^{5,39} J.M. Burward-Hoy,^{26,44} S. Butsyk,⁴⁴ X. Camard,⁴⁵ J.-S. Chai,¹⁸ P. Chand,⁴ W.C. Chang,² S. Chernichenko,¹⁵ C.Y. Chi,⁹ J. Chiba,²⁰ M. Chiu,⁹ I.J. Choi,⁵² J. Choi,¹⁹ R.K. Choudhury,⁴ T. Chujo,⁵ V. Cianciolo,³⁵ Y. Cobigo,¹⁰ B.A. Cole,⁹ P. Constantin,¹⁶ D. d'Enterria,⁴⁵ G. David,⁵ H. Delagrangé,⁴⁵ A. Denisov,¹⁵ A. Deshpande,³⁹ E.J. Desmond,⁵ A. Devismes,⁴⁴ O. Dietzsch,⁴¹ O. Drapier,²⁵ A. Drees,⁴⁴ K.A. Drees,⁵ R. du Rietz,²⁹ A. Durum,¹⁵ D. Dutta,⁴ Y.V. Efremenko,³⁵ K. El Chenawi,⁴⁹ A. Enokizono,¹⁴ H. En'yo,^{38,39} S. Esumi,⁴⁸ L. Ewell,⁵ D.E. Fields,^{33,39} F. Fleuret,²⁵ S.L. Fokin,²³ B.D. Fox,³⁹ Z. Fraenkel,⁵¹ J.E. Frantz,⁹ A. Franz,⁵ A.D. Frawley,¹² S.-Y. Fung,⁶ S. Garpman,^{29,*} T.K. Ghosh,⁴⁹ A. Glenn,⁴⁶ G. Gogiberidze,⁴⁶ M. Gonin,²⁵ J. Gosset,¹⁰ Y. Goto,³⁹ R. Granier de Cassagnac,²⁵ N. Grau,¹⁶ S.V. Greene,⁴⁹ M. Grosse Perdekamp,³⁹ W. Guryn,⁵ H.-Å. Gustafsson,²⁹ T. Hachiya,¹⁴ J.S. Haggerty,⁵ H. Hamagaki,⁸ A.G. Hansen,²⁷ E.P. Hartouni,²⁶ M. Harvey,⁵ R. Hayano,⁸ N. Hayashi,³⁸ X. He,¹³ M. Heffner,²⁶ T.K. Hemmick,⁴⁴ J.M. Heuser,⁴⁴ M. Hibino,⁵⁰ J.C. Hill,¹⁶ W. Holzmann,⁴³ K. Homma,¹⁴ B. Hong,²² A. Hoover,³⁴ T. Ichihara,^{38,39} V.V. Ikonnikov,²³ K. Imai,^{24,38} D. Isenhower,¹ M. Ishihara,³⁸ M. Issah,⁴³ A. Isupov,¹⁷ B.V. Jacak,⁴⁴ W.Y. Jang,²² Y. Jeong,¹⁹ J. Jia,⁴⁴ O. Jinnouchi,³⁸ B.M. Johnson,⁵ S.C. Johnson,²⁶ K.S. Joo,³¹ D. Jouan,³⁶ S. Kametani,^{8,50} N. Kamihara,^{47,38} J.H. Kang,⁵² S.S. Kapoor,⁴ K. Katou,⁵⁰ S. Kelly,⁹ B. Khachaturov,⁵¹ A. Khanzadeev,³⁷ J. Kikuchi,⁵⁰ D.H. Kim,³¹ D.J. Kim,⁵² D.W. Kim,¹⁹ E. Kim,⁴² G.-B. Kim,²⁵ H.J. Kim,⁵² E. Kistenev,⁵ A. Kiyomichi,⁴⁸ K. Kiyoyama,³² C. Klein-Boesing,³⁰ H. Kobayashi,^{38,39} L. Kochenda,³⁷ V. Kochetkov,¹⁵ D. Koehler,³³ T. Kohama,¹⁴ M. Kopytine,⁴⁴ D. Kotchetkov,⁶ A. Kozlov,⁵¹ P.J. Kroon,⁵ C.H. Kuberg,^{1,27} K. Kurita,³⁹ Y. Kuroki,⁴⁸ M.J. Kweon,²² Y. Kwon,⁵² G.S. Kyle,³⁴ R. Lacey,⁴³ V. Ladygin,¹⁷ J.G. Lajoie,¹⁶ A. Lebedev,^{16,23} S. Leckey,⁴⁴ D.M. Lee,²⁷ S. Lee,¹⁹ M.J. Leitch,²⁷ X.H. Li,⁶ H. Lim,⁴² A. Litvinenko,¹⁷ M.X. Liu,²⁷ Y. Liu,³⁶ C.F. Maguire,⁴⁹ Y.I. Makdisi,⁵ A. Malakhov,¹⁷ V.I. Manko,²³ Y. Mao,^{7,38} G. Martinez,⁴⁵ M.D. Marx,⁴⁴ H. Masui,⁴⁸ F. Matathias,⁴⁴ T. Matsumoto,^{8,50} P.L. McGaughey,²⁷ E. Melnikov,¹⁵ F. Messer,⁴⁴ Y. Miake,⁴⁸ J. Milan,⁴³ T.E. Miller,⁴⁹ A. Milov,^{44,51} S. Mioduszewski,⁵ R.E. Mischke,²⁷ G.C. Mishra,¹³ J.T. Mitchell,⁵ A.K. Mohanty,⁴ D.P. Morrison,⁵ J.M. Moss,²⁷ F. Mühlbacher,⁴⁴ D. Mukhopadhyay,⁵¹ M. Muniruzzaman,⁶ J. Murata,^{38,39} S. Nagamiya,²⁰ J.L. Nagle,⁹ T. Nakamura,¹⁴ B.K. Nandi,⁶ M. Nara,⁴⁸ J. Newby,⁴⁶ P. Nilsson,²⁹ A.S. Nyanin,²³ J. Nystrand,²⁹ E. O'Brien,⁵ C.A. Ogilvie,¹⁶ H. Ohnishi,^{5,38} I.D. Ojha,^{49,3} K. Okada,³⁸ M. Ono,⁴⁸ V. Onuchin,¹⁵ A. Oskarsson,²⁹ I. Otterlund,²⁹ K. Oyama,⁸ K. Ozawa,⁸ D. Pal,⁵¹ A.P.T. Palounek,²⁷ V. Pantuev,⁴⁴ V. Papavassiliou,³⁴ J. Park,⁴² A. Parmar,³³ S.F. Pate,³⁴ T. Peitzmann,³⁰ J.-C. Peng,²⁷ V. Peresedov,¹⁷ C. Pinkenburg,⁵ R.P. Pisani,⁵ F. Plasil,³⁵ M.L. Purschke,⁵ A.K. Purwar,⁴⁴ J. Rak,¹⁶ I. Ravinovich,⁵¹ K.F. Read,^{35,46} M. Reuter,⁴⁴ K. Reygers,³⁰ V. Riabov,^{37,40} Y. Riabov,³⁷ G. Roche,²⁸ A. Romana,²⁵ M. Rosati,¹⁶ P. Rosnet,²⁸ S.S. Ryu,⁵² M.E. Sadler,¹ N. Saito,^{38,39} T. Sakaguchi,^{8,50} M. Sakai,³² S. Sakai,⁴⁸ V. Samsonov,³⁷ L. Sanfratello,³³ R. Santo,³⁰ H.D. Sato,^{24,38} S. Sato,^{5,48} S. Sawada,²⁰ Y. Schutz,⁴⁵ V. Semenov,¹⁵ R. Seto,⁶ M.R. Shaw,^{1,27} T.K. Shea,⁵ T.-A. Shibata,^{47,38} K. Shigaki,^{14,20} T. Shiina,²⁷ C.L. Silva,⁴¹ D. Silvermyr,^{27,29} K.S. Sim,²² C.P. Singh,³ V. Singh,³ M. Sivertz,⁵ A. Soldatov,¹⁵ R.A. Soltz,²⁶ W.E. Sondheim,²⁷ S.P. Sorensen,⁴⁶ I.V. Sourikova,⁵ F. Staley,¹⁰ P.W. Stankus,³⁵ E. Stenlund,²⁹ M. Stepanov,³⁴ A. Ster,²¹ S.P. Stoll,⁵ T. Sugitate,¹⁴ J.P. Sullivan,²⁷ E.M. Takagui,⁴¹ A. Taketani,^{38,39} M. Tamai,⁵⁰ K.H. Tanaka,²⁰ Y. Tanaka,³² K. Tanida,³⁸ M.J. Tannenbaum,⁵ P. Tarján,¹¹ J.D. Tepe,^{1,27} T.L. Thomas,³³ J. Tojo,^{24,38} H. Torii,^{24,38} R.S. Towell,¹ I. Tseruya,⁵¹ H. Tsuruoka,⁴⁸ S.K. Tuli,³ H. Tydesjö,²⁹ N. Tyurin,¹⁵ H.W. van Hecke,²⁷ J. Velkovska,^{5,44} M. Velkovsky,⁴⁴ V. Veszprémi,¹¹ L. Villatte,⁴⁶ A.A. Vinogradov,²³ M.A. Volkov,²³ E. Vznuzdaev,³⁷ X.R. Wang,¹³ Y. Watanabe,^{38,39} S.N. White,⁵ F.K. Wohn,¹⁶ C.L. Woody,⁵ W. Xie,⁶ Y. Yang,⁷ A. Yanovich,¹⁵ S. Yokkaichi,^{38,39} G.R. Young,³⁵ I.E. Yushmanov,²³ W.A. Zajc,^{9,†} C. Zhang,⁹ S. Zhou,⁷ S.J. Zhou,⁵¹ and L. Zolin¹⁷

(PHENIX Collaboration)

¹Abilene Christian University, Abilene, TX 79699, USA

²Institute of Physics, Academia Sinica, Taipei 11529, Taiwan

³Department of Physics, Banaras Hindu University, Varanasi 221005, India

⁴Bhabha Atomic Research Centre, Bombay 400 085, India

⁵Brookhaven National Laboratory, Upton, NY 11973-5000, USA

⁶University of California - Riverside, Riverside, CA 92521, USA

⁷China Institute of Atomic Energy (CIAE), Beijing, People's Republic of China

- ⁸Center for Nuclear Study, Graduate School of Science, University of Tokyo, 7-3-1 Hongo, Bunkyo, Tokyo 113-0033, Japan
⁹Columbia University, New York, NY 10027 and Nevis Laboratories, Irvington, NY 10533, USA
¹⁰Dapnia, CEA Saclay, F-91191, Gif-sur-Yvette, France
¹¹Debrecen University, H-4010 Debrecen, Egyetem tér 1, Hungary
¹²Florida State University, Tallahassee, FL 32306, USA
¹³Georgia State University, Atlanta, GA 30303, USA
¹⁴Hiroshima University, Kagamiyama, Higashi-Hiroshima 739-8526, Japan
¹⁵Institute for High Energy Physics (IHEP), Protvino, Russia
¹⁶Iowa State University, Ames, IA 50011, USA
¹⁷Joint Institute for Nuclear Research, 141980 Dubna, Moscow Region, Russia
¹⁸KAERI, Cyclotron Application Laboratory, Seoul, Korea
¹⁹Kangnung National University, Kangnung 210-702, Korea
²⁰KEK, High Energy Accelerator Research Organization, Tsukuba-shi, Ibaraki-ken 305-0801, Japan
²¹KFKI Research Institute for Particle and Nuclear Physics (RMKI), H-1525 Budapest 114, POBox 49, Hungary
²²Korea University, Seoul, 136-701, Korea
²³Russian Research Center “Kurchatov Institute”, Moscow, Russia
²⁴Kyoto University, Kyoto 606-8502, Japan
²⁵Laboratoire Leprince-Ringuet, Ecole Polytechnique, CNRS-IN2P3, Route de Saclay, F-91128, Palaiseau, France
²⁶Lawrence Livermore National Laboratory, Livermore, CA 94550, USA
²⁷Los Alamos National Laboratory, Los Alamos, NM 87545, USA
²⁸LPC, Université Blaise Pascal, CNRS-IN2P3, Clermont-Fd, 63177 Aubiere Cedex, France
²⁹Department of Physics, Lund University, Box 118, SE-221 00 Lund, Sweden
³⁰Institut für Kernphysik, University of Muenster, D-48149 Muenster, Germany
³¹Myongji University, Yongin, Kyonggido 449-728, Korea
³²Nagasaki Institute of Applied Science, Nagasaki-shi, Nagasaki 851-0193, Japan
³³University of New Mexico, Albuquerque, NM 87131, USA
³⁴New Mexico State University, Las Cruces, NM 88003, USA
³⁵Oak Ridge National Laboratory, Oak Ridge, TN 37831, USA
³⁶IPN-Orsay, Université Paris Sud, CNRS-IN2P3, BP1, F-91406, Orsay, France
³⁷PNPI, Petersburg Nuclear Physics Institute, Gatchina, Russia
³⁸RIKEN (The Institute of Physical and Chemical Research), Wako, Saitama 351-0198, JAPAN
³⁹RIKEN BNL Research Center, Brookhaven National Laboratory, Upton, NY 11973-5000, USA
⁴⁰St. Petersburg State Technical University, St. Petersburg, Russia
⁴¹Universidade de São Paulo, Instituto de Física, Caixa Postal 66318, São Paulo CEP05315-970, Brazil
⁴²System Electronics Laboratory, Seoul National University, Seoul, Korea
⁴³Chemistry Department, Stony Brook University, SUNY, Stony Brook, NY 11794-3400, USA
⁴⁴Department of Physics and Astronomy, Stony Brook University, SUNY, Stony Brook, NY 11794, USA
⁴⁵SUBATECH (Ecole des Mines de Nantes, CNRS-IN2P3, Université de Nantes) BP 20722 - 44307, Nantes, France
⁴⁶University of Tennessee, Knoxville, TN 37996, USA
⁴⁷Department of Physics, Tokyo Institute of Technology, Tokyo, 152-8551, Japan
⁴⁸Institute of Physics, University of Tsukuba, Tsukuba, Ibaraki 305, Japan
⁴⁹Vanderbilt University, Nashville, TN 37235, USA
⁵⁰Waseda University, Advanced Research Institute for Science and Engineering, 17 Kikui-cho, Shinjuku-ku, Tokyo 162-0044, Japan
⁵¹Weizmann Institute, Rehovot 76100, Israel
⁵²Yonsei University, IPAP, Seoul 120-749, Korea
- (Dated: June 21, 2018)

A measurement of direct photons in p+p collisions at $\sqrt{s} = 200$ GeV is presented. A photon excess above background from $\pi^0 \rightarrow \gamma + \gamma$, $\eta \rightarrow \gamma + \gamma$ and other decays is observed in the transverse momentum range $5.5 < p_T < 7$ GeV/c. The result is compared to a next-to-leading-order perturbative QCD calculation. Within errors, good agreement is found between the QCD calculation and the measured result.

PACS numbers: 13.85.Qk, 25.75.Dw

Measurements of particle production at large transverse momenta (p_T) in hadronic interactions provide the

possibility to test perturbative quantum chromodynamics (pQCD). Neutral-pion production in p+p collisions at $\sqrt{s} = 200$ GeV in the range $2 < p_T < 13$ GeV/c measured by the PHENIX experiment at RHIC can be well described by next-to-leading-order (NLO) pQCD [1]. This comparison, however, relies on the choice of the parton-to-pion fragmentation function. Measurement of

*Deceased

†PHENIX Spokesperson: zajc@nevis.columbia.edu

direct-photon production provides a more direct test of pQCD. Quark-antiquark annihilation ($q\bar{q} \rightarrow \gamma g$) and quark-gluon Compton scattering ($qg \rightarrow q\gamma$) contribute to direct-photon production at leading order [2]. Due to the latter process, which dominates the production, the measurement of direct photons can be used to obtain information on the parton distribution function of the gluon inside the proton.

Previous direct-photon measurements in p+p collisions were made up to energies of $\sqrt{s} = 63$ GeV (see *e.g.* [3, 4, 5]). For p + \bar{p} collisions direct-photon data are available at considerably higher energies, $\sqrt{s} = 546, 630$ GeV [6, 7, 8] up to $\sqrt{s} = 1800$ GeV [9, 10]. At these energies NLO pQCD calculations describe the direct-photon data within about 20%, although systematic differences in the spectral shapes were observed [11]. At energies below $\sqrt{s} = 63$ GeV the agreement between NLO pQCD and data is generally worse. With phenomenological approaches based on soft-gluon radiation of the incoming parton, which leads to an additional transverse momentum k_T , a better description of the data can be obtained [12]. The Relativistic Heavy Ion Collider (RHIC) at the Brookhaven National Laboratory provides p+p collisions at energies between the existing data sets, allowing better constraints on the processes affecting incoming partons. A further incentive to study direct-photon production in p+p at $\sqrt{s} = 200$ GeV comes from the measurement of direct photons in collisions of gold nuclei at the same center-of-mass energy per nucleon-nucleon pair [13, 14]. In central Au+Au collisions high- p_T neutral-pion production is suppressed [15] which is due to energy loss of the scattered quarks and gluons in the hot and dense fireball created in these collisions (jet quenching) [16]. As direct photons are not subject to the strong interaction they should not be suppressed in the jet-quenching model. In this context, the p+p direct-photon results serve as a baseline against which possible nuclear effects can be identified.

The data presented in this report were collected during the 2001-2002 run period (Run 2) of RHIC. The neutral-pion cross sections obtained from this data set were published in [1]. The unpolarized neutral-pion spectrum and the unpolarized direct-photon spectrum presented here were obtained by averaging over proton bunches with varying vertical polarization delivered by RHIC.

Direct photons and background photons from decays $\pi^0 \rightarrow \gamma + \gamma$ and $\eta \rightarrow \gamma + \gamma$ were measured with the electromagnetic calorimeter (EMCal) of the PHENIX experiment [17]. The background from charged particles was subtracted with the aid of a layer of multi-wire proportional chambers with pad readout (PC3) which was located directly in front of the EMCal. The minimum-bias trigger was provided by two beam-beam counters (BBC) which were also used to determine the collision vertex. In addition to the minimum-bias trigger conditions, a high- p_T photon trigger was used, derived from the analog energy signal measured with the EMCal.

The two BBC's were located symmetrically around the

nominal interaction point at ± 1.44 m along the beamline. The BBC's subtended the pseudorapidity range $\pm (3.1 - 3.9)$ with full azimuthal coverage. The collision vertex was determined by measuring the difference of particle arrival times in the two BBC's. This analysis was restricted to events with a vertex in the range ± 30 cm. The BBC's were calibrated as a luminosity detector with absolute luminosity measurements based on the van der Meer scan technique [18]. With these scans the cross section for firing the BBC minimum-bias trigger was determined to be 21.8 ± 2.1 mb [1]. Thus, roughly 50% of the inelastic p+p events satisfy the minimum-bias trigger condition if an inelastic p+p cross section of 42 mb at $\sqrt{s} = 200$ GeV is assumed.

The PHENIX EMCal comprises two arms each with 4 sectors [19]. The EMCal consists of two different sub-detectors, a lead-scintillator calorimeter (PbSc, 6 sectors) and a lead-glass calorimeter (PbGl, 2 sectors). Each sector covers a pseudorapidity range of $|\eta| < 0.35$ and an azimuthal range of $\Delta\phi \approx 22.5^\circ$. Each PbSc (PbGl) sector is highly segmented and consists of 72×36 (96×48) individual detector modules, called towers, with a lateral size of 5.5×5.5 cm² (4×4 cm²). With a radial distance of the sectors to the beamline of roughly 5 m this corresponds to a segmentation of $\Delta\phi \times \Delta\eta \approx 0.01 \times 0.01$ such that the two decay photons of a π^0 are well separated up to neutral-pion momenta of $p_T \approx 20$ GeV/ c . The different detection mechanisms of the two sub-detectors (measurement of scintillation light in PbSc and detection of Cherenkov photons in PbGl) result in a different response to hadrons. Thus, the PbSc and PbGl provide photon measurements with different systematic uncertainties. The energy calibration of the detector was obtained from the position of the π^0 invariant-mass peaks. A $\sim 4\%$ ($\sim 5\%$) shift of the π^0 peak position due to energy smearing in conjunction with the influence of the steeply falling π^0 p_T spectrum was taken into account in the PbSc (PbGl) calibration. The calibration was corroborated by correlating the EMCal energy with the momentum of electrons measured with the PHENIX tracking detectors and, in case of the PbSc, by measuring the energy deposited by minimum-ionizing particles. From these studies the systematic uncertainty of the energy measurement was estimated to be less than 1.5%. In a direct-photon analysis it is essential to exclude bad detector modules ("hot towers") which might give rise to spurious direct-photon signals. A detailed quality assessment was carried out to identify such towers.

The EMCal high- p_T trigger (called 2×2) was based on the analog energy signal measured in 2×2 groups of adjacent EMCal towers (called trigger tiles). The average threshold of the trigger corresponded to an energy signal of 0.75 GeV. The probability as a function of the photon p_T to fire the trigger was determined by Monte Carlo simulations which included the variation of the trigger tile thresholds, the EMCal detector response, and the geometry of the active trigger tiles. This trigger efficiency was confirmed with minimum-bias data. The

photon trigger efficiencies for PbSc and PbGl reached a plateau above $p_T = 1.5 - 2$ GeV/ c at the limit of about 0.78 expected from the number of active towers and 2×2 trigger tiles. The high- p_T -trigger photon sample was used above $p_T = 3$ GeV/ c in the final spectrum.

Another EMCal trigger which did not require a coincidence with the minimum-bias trigger was used to account for the bias on the particle measurement due to the minimum-bias event selection. To this end the fraction of π^0 's measured with this EMCal trigger for events which in addition satisfied the minimum-bias trigger condition was determined to be $f = 0.75 \pm 0.02$. The unbiased photon and neutral pions cross sections were then determined by dividing the total number of measured photons and neutral pions by this number.

The minimum-bias data sample in this analysis consisted of 16.7 million events, corresponding to an integrated luminosity of 0.77 nb^{-1} . About 1 in 47 minimum-bias events also satisfied the 2×2 high- p_T trigger condition. The 18.7 million analyzed 2×2 events thus corresponded to an integrated luminosity of 40.3 nb^{-1} .

The first step in the direct-photon analysis was to define a sample of direct-photon-candidate hits. An EMCal hit was rejected as a direct-photon candidate if it formed an invariant mass in the π^0 or η range with other hits in the same or adjacent sectors. The invariant-mass window was $110 < m_{\gamma\gamma} < 170 \text{ MeV}/c^2$ for the π^0 and $500 < m_{\gamma\gamma} < 620 \text{ MeV}/c^2$ for the η , corresponding roughly to a $\pm 2\sigma$ window around the observed π^0 and η peaks. To keep the rate of accidental rejections of genuine direct photons low it was required that the partner hits had a transverse momentum of $p_T > 0.4 \text{ GeV}/c$. This cut effectively corresponded to a p_T -dependent upper limit on the energy asymmetry $\alpha = |E_{\gamma 1} - E_{\gamma 2}| / (E_{\gamma 1} + E_{\gamma 2})$ in the rejection procedure. In spite of this requirement, a small fraction of genuine direct photons is rejected. This was studied by inserting artificially generated direct-photon hits into real events. In order to keep the hit multiplicity constant, a randomly selected real hit was removed from an event in this procedure. It was found that the loss of genuine direct photons was less than 2% for $p_T > 3 \text{ GeV}/c$. The final direct-photon spectrum was corrected for this effect. In order to increase the chances of finding the partner photon for a π^0 or η decay photon, direct-photon candidates were required to lie within a restricted fiducial area which was defined by a minimum distance of 16 (20) towers to the edge of the detector for the PbSc (PbGl). For example, for π^0 's with $p_T = 4 \text{ GeV}/c$ and the requirement that one decay photon has a $p_T > 0.4 \text{ GeV}/c$ the average distance of the decay photons in tower units is ~ 8 (~ 11) for PbSc (PbGl). With the chosen fiducial area basically all decay photons from neutral pions with $p_T \gtrsim 4 \text{ GeV}/c$ can be tagged. Monte Carlo studies showed that the rejection of direct-photon candidates based on the π^0 and η tagging lead to a reduction of background photons from hadron decays in the fiducial area of about a factor of 2 for $p_T > 5 \text{ GeV}/c$. Some direct-photon analyses only

measure isolated direct photons for which the total transverse energy or the number of charged tracks in a cone centered around the direct photon is required to lie below a threshold. No such cut was used in this analysis.

In order to reduce the background from hadronic hits in the EMCal, cuts were applied on the lateral shower shape and on the time-of-flight of the hits. The remaining contamination of charged particles was subtracted on a statistical basis by employing the PC3 as a charged-particle veto detector. The intrinsic efficiency of the PC3 for detecting a charged particle was higher than 99% and the active PC3 area in the EMCal acceptance was roughly 90%. PC3 hits were projected onto the EMCal surface using a straight line given by the PC3 hit and the event vertex. An EMCal hit within a certain veto radius was counted as a charged hit. The chosen veto radius decreased with increasing p_T and for $p_T > 0.8 \text{ GeV}/c$ a constant value of 15 cm was used. The fraction of charged hits was corrected for random associations with the help of a mixed-event technique. The charged-particle background in the direct-photon-candidate sample was $\sim 15\%$ around $p_T = 5 \text{ GeV}/c$ for both PbSc and PbGl. A large fraction of these background hits, however, comes from photon conversion in the field-free region between the vertex and PC3. The photon loss due to conversion was calculated based on the material budget up to PC3. The photon conversion probability was 4.1% for the 2 PbSc sectors in the East Arm of the central spectrometer, 5.3% for the 4 sectors in the West Arm, and 7.4% for the PbGl. These conversion losses were taken into account in the final photon cross section. The correction for the contamination of the raw spectrum of neutral EMCal hits with neutrons and anti-neutrons was determined with a detailed GEANT simulation [20]. In the case of the PbGl calorimeter the simulation was based on the creation of Cherenkov photons in order to achieve a realistic description of the detector response. The background from neutral particles was found to decrease with p_T and was already less than 1% for $p_T > 2 \text{ GeV}/c$ for both PbSc and PbGl.

The geometric acceptance and the efficiency of the photon detection were calculated with a Monte Carlo simulation. The efficiency takes the distortion of the direct-photon-candidate spectrum due to energy smearing into account. Moreover, it corrects the small ($\lesssim 5\%$) loss of photons due to the shower shape and time-of-flight cuts. The final direct-photon spectrum was corrected for the difference between the average direct-photon cross section within a finite p_T bin and the value of the cross section at the bin center.

With the described corrections the unbiased differential cross section $\gamma_{\text{direct}}^{\text{cand}} \equiv E d^3\sigma/d^3p$ for the direct-photon candidates calculated from the minimum bias data sample reads

$$E \frac{d^3\sigma}{d^3p} = \frac{1}{\hat{\mathcal{L}}} \cdot \frac{1}{2\pi p_T} \cdot \frac{C_{\text{reco}} \cdot C_{\text{conv}} \cdot C_{\text{loss}}}{f} \cdot \frac{N_{\text{direct}\gamma}^{\text{cand}}}{\Delta p_T \cdot \Delta y} \quad (1)$$

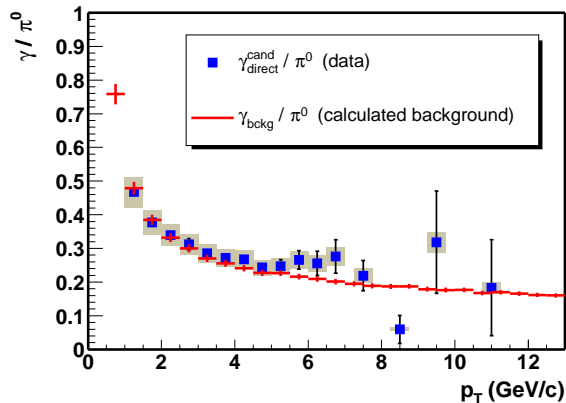


FIG. 1: (color online) Ratio of direct-photon candidates to the π^0 spectrum. The histogram represents the expected background signal from the Monte Carlo calculation. The error bars represent the statistical error and the boxes the systematic error.

TABLE I: Systematic uncertainties of the neutral-pion spectrum, the direct-photon-candidate spectrum, and the measured and simulated γ/π^0 ratios at $p_T = 6.75$ GeV/c.

π^0 error source	PbGl	PbSc
Yield extraction	5%	5%
Yield correction	8%	6%
Energy scale	9%	8%
Total	13%	12%
$\gamma_{\text{direct}}^{\text{cand}}$ error source	PbGl	PbSc
Non- γ background correction	4%	4%
Yield correction	6%	5%
Energy scale	9%	9%
Total	12%	11%
Total error	PbGl+PbSc combined	
$\gamma_{\text{direct}}^{\text{cand}}/\pi^0$	9%	
$\gamma_{\text{bckg}}/\pi^0$	4%	

where $N_{\text{direct}\gamma}^{\text{cand}}$ is the total number of direct-photon candidates in a p_T bin Δp_T and rapidity bin Δy ; C_{reco} is the acceptance and efficiency correction for photons; C_{conv} is the correction for photon conversions; C_{loss} is the correction for the loss of genuine direct photons in the π^0 and η tagging; $f = 0.75 \pm 0.02$ is the fraction of the unbiased direct photon yield which is measured under the minimum bias trigger condition; and $\hat{\mathcal{L}}$ is the integrated luminosity for the analyzed data sample. The high- p_T triggered sample required an additional correction for the efficiency of this trigger for photon detection.

The p_T spectrum of the direct-photon candidates contains direct photons as well as remaining background photons from hadron decays. These background photons mostly come from π^0 and η decays for which one

decay photon misses the detector. At a representative bin of $p_T = 6.75$ GeV/c about 93% of the background photons originate from π^0 and η decays, the remaining background photon come from decays of other hadrons like ω and η' . The background was calculated with the same Monte Carlo code that was used for the acceptance and efficiency calculation. The Monte Carlo code took a parameterization of the measured π^0 spectrum as input. The spectra of η mesons and other hadrons with photon decay branches were assumed to have the same shape as the π^0 spectrum as a function of $m_T = \sqrt{p_T^2 + m_0^2}$ (m_T scaling [21, 22]). The η/π^0 invariant cross section ratio as a function of m_T was taken as 0.48 ± 0.1 which was confirmed by the measured η spectrum.

The dominant systematic uncertainty of the neutral-pion spectrum and the direct-photon-candidate spectrum came from the uncertainty of the energy scale and the uncertainty of the yield correction. At $p_T = 6.75$ GeV/c, the 1.5% uncertainty of the energy scale resulted in a 9% uncertainty in the photon yield. The yield correction included the correction for energy and position smearing of the detector, for photon losses due to particle-identification cuts, for photon conversions, and for the detector acceptance. For the neutral pions an additional 5% uncertainty came from the extraction of the π^0 -peak content. In the case of the photon measurement the uncertainty due to the subtraction of charged and neutral backgrounds was taken into account. In the ratio $\gamma_{\text{direct}}^{\text{cand}}/\pi^0$ of the direct-photon-candidate spectrum and the neutral-pion spectrum systematic uncertainties partially cancel. Monte Carlo studies showed that the uncertainty of this ratio at $p_T = 6.75$ GeV/c due to a possible non-linearity of the energy scale was $\sim 2\%$.

For the determination of the direct-photon spectrum the expected background photons from hadronic decays need to be subtracted from the spectrum of direct-photon candidates. To this end the ratio $R_\gamma = (\gamma_{\text{direct}}^{\text{cand}}/\pi^0)/(\gamma_{\text{bckg}}/\pi^0)$ of the measured direct-photon candidates to the calculated background was determined. The direct-photon spectrum was then calculated as

$$\gamma_{\text{direct}} = (1 - R_\gamma^{-1}) \cdot \gamma_{\text{direct}}^{\text{cand}}. \quad (2)$$

The relative systematic uncertainty of the direct-photon cross section was calculated as the quadratic sum of the relative uncertainties of the two factors in Eq. 2. The factor $1 - R_\gamma^{-1}$ contains the (statistical and systematic) significance of the direct photon signal. When multiplying with $\gamma_{\text{direct}}^{\text{cand}}$, only the systematic uncertainties that cancelled in the ratio R_γ are added (*e.g.* the energy scale error). The overall normalization uncertainty from the luminosity determination was 9.6%. The estimated systematic uncertainties for the measured neutral-pion spectrum and the measured direct-photon-candidate spectrum are shown in Table I for a representative bin ($p_T = 6.75$ GeV/c) of the spectrum. The systematic uncertainty of the direct-photon measurement was corroborated by comparing results obtained for the dif-

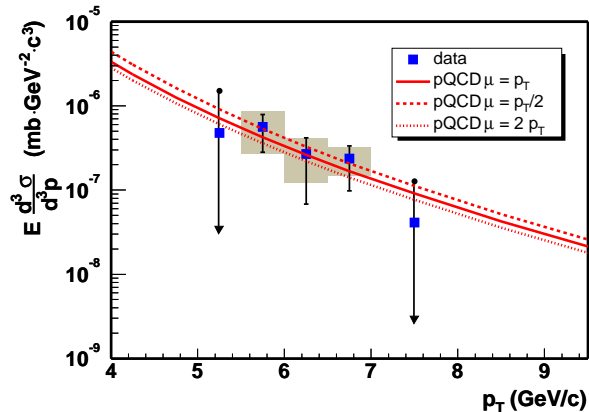


FIG. 2: (color online) Measured cross section and NLO pQCD calculations for direct-photon production in p+p collisions at $\sqrt{s} = 200$ GeV. The normalization error of 9.6% is not shown. The two data points plotted with an arrow indicate the beginning of the low- and high- p_T ranges where the direct photon signal is consistent with zero. The upper edges of the arrows indicate an upper limit (90% confidence level) for the direct photon cross section calculated from the statistical and systematic uncertainty.

TABLE II: Invariant differential cross section for direct-photon production in p+p collisions at $\sqrt{s} = 200$ GeV. Asymmetric uncertainties (σ_{low} , σ_{high}) are given for the cross section. The absolute normalization error of 9.6% is not included.

p_T (GeV/c)	$E d^3\sigma/d^3p$ (mb GeV $^{-2}$ c 3)	stat. error		sys. error	
		σ_{low}	σ_{high}	σ_{low}	σ_{high}
5.75	$5.61 \cdot 10^{-7}$	50 %	42 %	53 %	54 %
6.25	$2.68 \cdot 10^{-7}$	75 %	56 %	55 %	56 %
6.75	$2.37 \cdot 10^{-7}$	59 %	42 %	37 %	38 %

ferent photon-identification criteria. Moreover, the individual PbG1 and PbSc results were found to agree within systematic errors.

To make the best use of the available Run-2 statistics the photon and π^0 spectra from PbSc and PbG1 were combined for the final result. The ratio of the acceptance- and efficiency-corrected direct-photon candidate p_T spectrum to the measured π^0 spectrum is depicted in Fig. 1. In addition, the Monte Carlo calculation for the ratio of the expected background photons to the π^0 spectrum is shown. At high p_T the statistical significance of the direct-photon-candidate spectrum is weak. However, around $p_T \approx 6-7$ GeV/c there is clear evidence of a photon signal above the background.

The extracted invariant direct-photon spectrum is

shown in Fig. 2 and the numerical values are given in Table II. The experimental result was compared to NLO pQCD calculations [23, 24, 25, 26, 27, 28] which used the CTEQ6 parton distribution functions [29] and the GRV parton-to-photon fragmentation function [30]. There are in general two mechanisms for the production of direct photons: the direct contribution from elementary scattering processes of quarks and gluons, described in the introduction, and the contribution from photons which are produced in the fragmentation of quark or gluon jets. The latter is a long-distance process which is not perturbatively calculable. It is described by a parton-to-photon fragmentation function which is determined experimentally. Since no isolation cut was used in the data analysis the pQCD calculation in Fig. 2 includes contributions from the direct production mechanism and the fragmentation mechanism. The separation of short-distance and long-distance processes in the pQCD calculation introduces unphysical renormalization, factorization, and fragmentation scales. Identical values for all three scales were used in the pQCD calculation. In Fig. 2, results are shown for three choices of the scales ($\mu = p_T$, $\mu = p_T/2$, and $\mu = 2p_T$). The theoretical and experimental results agree within the large uncertainties of the data points.

Prior to the Run-2 p+p beamtime PHENIX took data from Au+Au collisions at $\sqrt{s_{NN}} = 200$ GeV. A clear direct-photon signal was observed in mid-central and central Au+Au reactions [13]. The strong suppression of π^0 's and η 's in Au+Au significantly reduced the number of background photons and eased the extraction of the direct-photon signal. The p+p NLO pQCD was used as a baseline reference for the interpretation of the Au+Au result. In contrast to neutral pions no sign of a suppression of direct photons in Au+Au collisions was found. The direct-photon measurement presented in this paper supports the use of the NLO pQCD calculation as a reference for the results measured in Au+Au.

In summary, a small but significant direct-photon signal has been observed at mid-rapidity in p+p collisions at $\sqrt{s} = 200$ GeV. The measured direct-photon cross section is in agreement with pQCD calculation, albeit within large errors.

We thank the staff of the Collider-Accelerator and Physics Departments at BNL for their vital contributions. We acknowledge support from the Department of Energy and NSF (U.S.A.), MEXT and JSPS (Japan), CNPq and FAPESP (Brazil), NSFC (China), CNRS-IN2P3 and CEA (France), BMBF, DAAD, and AvH (Germany), OTKA (Hungary), DAE and DST (India), ISF (Israel), KRF and CHEP (Korea), RMIST, RAS, and RMAE (Russia), VR and KAW (Sweden), U.S. CRDF for the FSU, US-Hungarian NSF-OTKA-MTA, and US-Israel BSF.

[1] S. S. Adler et al. (PHENIX), Phys. Rev. Lett. **91**, 241803 (2003), hep-ex/0304038.

[2] H. Fritzsche and P. Minkowski, Phys. Lett. **B69**, 316

- (1977).
- [3] E. Anassontzis et al., *Zeit. Phys.* **C13**, 277 (1982).
 - [4] L. Apanasevich (Fermilab E706) (2004), hep-ex/0407011.
 - [5] G. Ballocci et al. (UA6), *Phys. Lett.* **B436**, 222 (1998).
 - [6] C. Albajar et al. (UA1), *Phys. Lett.* **B209**, 385 (1988).
 - [7] R. Ansari et al. (UA2), *Z. Phys.* **C41**, 395 (1988).
 - [8] J. Alitti et al. (UA2), *Phys. Lett.* **B263**, 544 (1991).
 - [9] F. Abe et al. (CDF), *Phys. Rev. Lett.* **73**, 2662 (1994).
 - [10] B. Abbott et al. (D0), *Phys. Rev. Lett.* **84**, 2786 (2000), hep-ex/9912017.
 - [11] D. Acosta et al. (CDF), *Phys. Rev.* **D65**, 112003 (2002), hep-ex/0201004.
 - [12] L. Apanasevich et al., *Phys. Rev.* **D59**, 074007 (1999), hep-ph/9808467.
 - [13] J. Frantz (PHENIX), *J. Phys.* **G30**, S1003 (2004), nucl-ex/0404006.
 - [14] S. S. Adler et al. (PHENIX), to be submitted to *Phys. Rev. Lett.* (2005).
 - [15] S. S. Adler et al. (PHENIX), *Phys. Rev. Lett.* **91**, 072301 (2003), nucl-ex/0304022.
 - [16] M. Gyulassy, I. Vitev, X.-N. Wang, and B.-W. Zhang (2003), nucl-th/0302077.
 - [17] K. Adcox et al. (PHENIX), *Nucl. Instrum. Meth.* **A499**, 469 (2003).
 - [18] S. van der Meer, CERN Internal Report ISR-PO/68-31 (1968).
 - [19] L. Aphecetche et al. (PHENIX), *Nucl. Instrum. Meth.* **A499**, 521 (2003).
 - [20] *Geant 3.21*, CERN program library.
 - [21] B. Alper et al. (British-Scandinavian), *Nucl. Phys.* **B87**, 19 (1975).
 - [22] K. Alpgard et al. (UA5), *Phys. Lett.* **B107**, 310 (1981).
 - [23] L. E. Gordon and W. Vogelsang, *Phys. Rev.* **D48**, 3136 (1993).
 - [24] L. E. Gordon and W. Vogelsang, *Phys. Rev.* **D50**, 1901 (1994).
 - [25] P. Aurenche, A. Douiri, R. Baier, M. Fontannaz, and D. Schiff, *Phys. Lett.* **B140**, 87 (1984).
 - [26] P. Aurenche, R. Baier, M. Fontannaz, and D. Schiff, *Nucl. Phys.* **B297**, 661 (1988).
 - [27] H. Baer, J. Ohnemus, and J. F. Owens, *Phys. Lett.* **B234**, 127 (1990).
 - [28] H. Baer, J. Ohnemus, and J. F. Owens, *Phys. Rev.* **D42**, 61 (1990).
 - [29] J. Pumplin et al., *JHEP* **07**, 012 (2002), hep-ph/0201195.
 - [30] M. Gluck, E. Reya, and A. Vogt, *Phys. Rev.* **D48**, 116 (1993), erratum *ibid.* **D51**, 1427 (1995).